Microwave System for Head Imaging

Beada'a J. Mohammed, Amin M. Abbosh, *Senior Member, IEEE*, Samah Mustafa, and David Ireland

***Abstract*— A wideband microwave system for head imaging is presented. The system includes an array of 16 corrugated tapered slot antennas that are installed on an adjustable platform. A switching device is used to enable the antennas to sequentially send a wideband 1–4 GHz microwave signal and capture the backscattered signals. Those signals are recorded using suitably designed virtual instrument software architecture. To test the capability of the system to detect brain injuries, a low-cost mixture of materials that emulate the frequency-dispersive electrical properties of the major brain tissues across the frequency band 1–4 GHz are used to construct a realistic-shape head phantom. A target that emulates a realistic hemorrhage stroke is fabricated and inserted in two different locations inside the fabricated head phantom. A preprocessing algorithm that utilizes the symmetry of the two halves of human head is used to extract the target response from the background reflections. A post-processing confocal algorithm is used to get an image of the phantom and to accurately detect the presence and location of the stroke.**

***Index Terms*— Brain imaging, microwave imaging.**

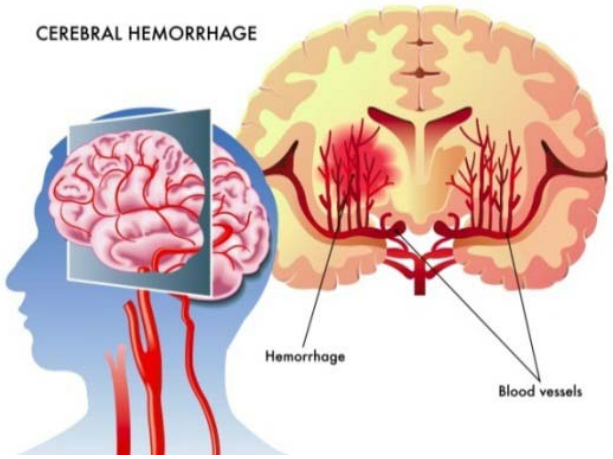

Fig. 1. Illustration of cerebral hemorrhage stroke forming a pool of blood inside the brain.

I. Introduction

MICROWAVE imaging has been widely used in many civil, industrial, and medical applications, such as nondestructive testing, materials characterization, remote sensing, and medical diagnosis [1]–[21]. Microwave imaging techniques in those and many other applications are utilized due to the capability of microwave frequency bands to penetrate inside dielectric materials. The scattered or reflected signals from those materials are measured and processed to get a useful image of the target. The principle of operation of microwave imaging systems is the contrast in the electrical properties between various parts of the imaged object and its surroundings.

In medical applications, there has been a huge interest in using microwave imaging techniques for the detection of tissues' abnormality, such as breast cancer and brain stroke [6]–[21]. The main motivation for that interest is to build a low-cost, nonionizing imaging system that can replace or complement the available diagnostic tools.

Manuscript received December 2, 2012; revised March 30, 2013; accepted April 29, 2013. Date of publication August 30, 2013; date of current version December 5, 2013. The Associate Editor coordinating the review process was Dr. Matteo Pastorino.

B. J. Mohammed is with the University of Queensland, Brisbane 4072, Australia, and also with the College of Electronics Engineering, Mosul University, Mosul 09334, Iraq (e-mail: b.mohammed@uq.edu.au).

A. M. Abbosh, and S. Mustafa are with the University of Queensland, Brisbane 4072, Australia (e-mail: a.abbosh@uq.edu.au; samah.mustafa@uq.edu.au).

D. Ireland is with the Information and Communication Technologies Division, CSIRO, Queensland 4069, Australia (e-mail: d.ireland@csiro.au).

Color versions of one or more of the figures in this paper are available online at http://ieeexplore.ieee.org.

Digital Object Identifier 10.1109/TIM.2013.2277562

There are many research groups around the globe working on designing microwave systems for breast imaging [6]–[10]; however, hitherto there have been limited efforts to build a complete microwave system for head imaging. Currently, the clinical imaging diagnosis tools used to detect brain injuries are the computed tomography, magnetic resonant imaging scanning, positron emission tomography, and ultrasound.

The main aims of head imaging are to detect the presence and location of damaged brain tissues that are caused by different medical conditions or injuries, such as ischemic or hemorrhagic brain strokes [11]–[22]. An illustration of a cerebral hemorrhagic stroke is shown in Fig. 1. This form of stroke is caused by a burst blood vessel that forms a pool of blood that compresses the brain tissues and eventually causes death. There is a potential to use microwave systems for brain imaging because of the high contrast in the electric properties between the healthy and stroke-affected brain tissues. By being low-cost, portable, and utilizing nonionizing radiation, a microwave system for brain imaging could be an important tool for a first response ambulance team whose actions are critical to the patient's recovery. Moreover, that system could be a significant addition to existing stroke diagnostic tools.

Reviewing the literature shows that most of the efforts concerning microwave imaging of human brain rely on computer simulations that are based on numerical head phantoms derived from MRI scans [11]–[17]. Experiments, involving microwave imaging of realistic head phantoms occur infrequently in the literature. Those experiments involve using over-simplified systems and head phantoms [18]–[22]. As such, there is a need to develop a complete experimental microwave imaging

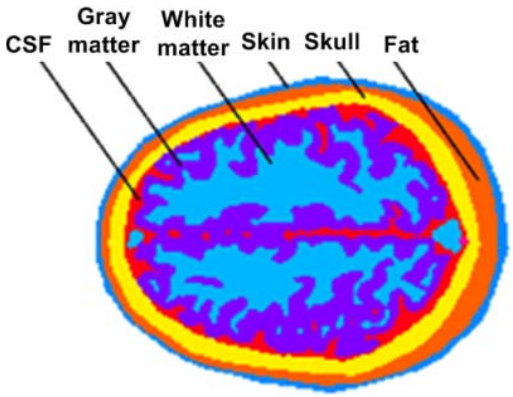

Fig. 2. Main tissues in human brain.

system that is dedicated to human brain imaging. The availability of such a system is important to test different techniques and methods that might help to realize building a successful preclinical head imaging system. Moreover, the fabrication of a realistic head phantom that includes the main tissues of human brain depicted in Fig. 2 is also needed to test the proposed system.

This paper presents the design and development of a microwave system that can be used for head imaging. In case of head injuries, the system can be used to find the position and extent of the affected brain tissues. It can thus be utilized for the immediate diagnosis of a major medical condition: brain stroke. The immediate stroke detection leads to an immediate proper treatment, which can eventually save lives and reduce disability rates.

The proposed system operates across the wideband frequency range from 1 GHz to 4 GHz. This frequency range is chosen as it covers the bands that offer a reasonable compromise between the required head penetration of low-power microwave signals and acceptable image resolution [13]. To demonstrate the capabilities of the designed system, it is used to detect and locate a target emulating a hemorrhagic stroke in a realistic head phantom that is also explained in this paper.

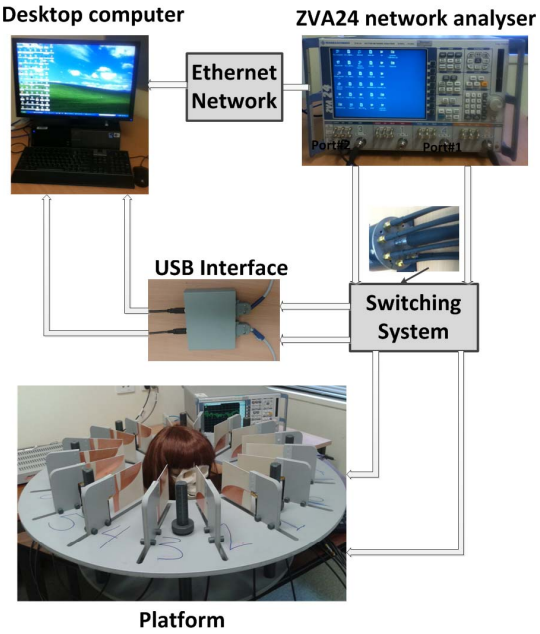

(a)

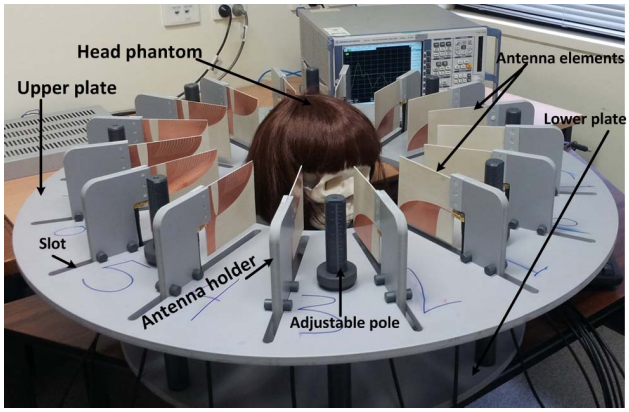

(b)

Fig. 3. (a) Configuration of the whole microwave imaging system. (b) Details of the platform.

II. Elements of the Imaging System

A microwave system to test the feasibility of using microwaves for head imaging is built as shown in Fig. 3. The designed imaging system operates across the frequency band from 1 GHz to 4 GHz. The system includes a semielliptical array of 16 antenna elements that are installed on an adjustable platform, data acquisition unit, head phantom, vector network analyzer, and computer. The details of each of those units are given in the following sections.

A. Antenna Array

In order to achieve wideband operation, the utilized antenna array in the system employs tapered slot antenna elements. The utilized antennas have directional radiation patterns, which is an important factor in the biomedical applications, as the allowed microwave power level is limited. Special considerations are given to their compact size without compromising their directional properties and distortion-less pulse transmission. These goals are fulfilled using high dielectric substrate materials and suitably chosen shapes of corrugations in the metallic parts. For the proposed system, the antenna array is required to operate in free-space. Since the purpose of the antenna is to transmit/ receive the band from 1 GHz to 4 GHz, the reflection coefficient (S11) less than -10 dB over the frequency range of interest is required.

The geometry and the detailed parameters of the proposed wideband exponentially corrugated tapered slot antenna are shown in Fig. 4. The first step in the design is the radiating structure of the antenna, which is in the form of antipodal configuration. The width of the antenna $(W+2W_d)$ is determined by assuming it equal to half of the effective wavelength at the lowest frequency of operation (1 GHz). The slot flare of the radiators is tapered exponentially. The ground plane of the microstrip is tapered elliptically for the transition from the input microstrip feeder to the antenna's parallel-strip feeder.

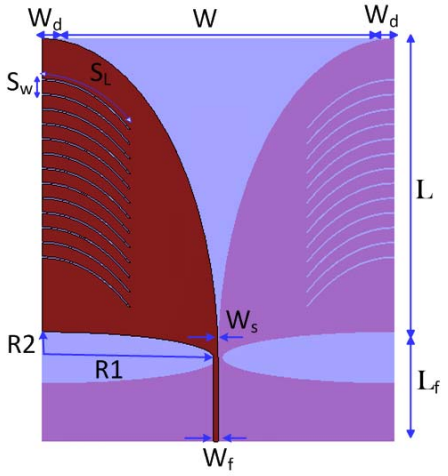

Fig. 4. Configuration of the antenna.

The major and secondary radii of this ellipse are chosen using the guidelines presented in [23].

Next, the symmetrical exponential corrugations are introduced in the radiator to enable the antenna to resonate at a low frequency without the need to use large-size structure. The depth of the corrugations is chosen to be less than quarter of the effective wavelength at the lowest frequency of operation. The chosen depth for the slots presents an inductive reactance to the passing wave, and thus increases the effective electric length of the structure [24]. Therefore, the corrugated radiator with those short circuited slots resonates at a lower frequency, as compared with the noncorrugated structure.

The CST Microwave Studio is used to find the optimum opening rate of the slot flare, the slot width, and the width of the microstrip line. The optimization process is configured to achieve a reflection coefficient below -10 dB and a front-to-back ratio higher than 10 dB across the band of interest. The dimensions of the antenna using the substrate Rogers RO3010 with dielectric constant $= 10.2$ and thickness $= 1.28$ mm are W $= 90$ mm, $W_d = 2$ mm, L $= 95$ mm, $L_f = 15$ mm, R1 $=$ 43.8 mm, R2 $= 8.7$ mm, and $W_f = 1.189$ mm. The slots used for the corrugations have a length $S_L = 43.5$ mm, whereas the space between each neighboring pair of slots is $S_w = 1$ mm.

The performance of the utilized antenna is verified using CST Microwave Studio, and measurements. As depicted in Fig. 5, the antenna has less than -10 dB reflection coefficient across the utilized band. To test the ability of the antenna to transmit and receive wideband microwave signals without distortion, two identical antennas are placed facing each other with 40 cm distance between them. The transmitted and received pulses are normalized. The result shown in Fig. 6 indicates a low distortion in the received pulses.

The required semielliptical antenna array is formed using 16 antenna elements. The distance between neighboring antenna elements in the array is optimized for less than -20 dB of mutual coupling (S12) as depicted in Fig. 7. The optimized space is 6 cm.

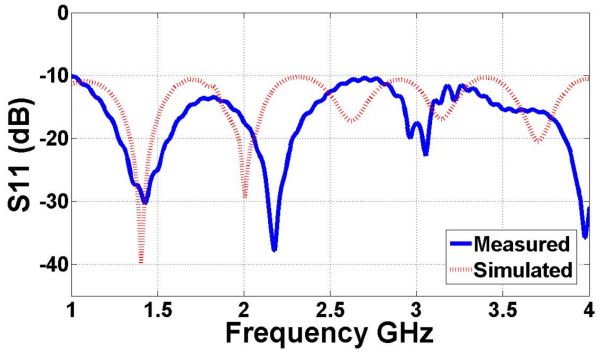

Fig. 5. Reflection coefficient of the antenna.

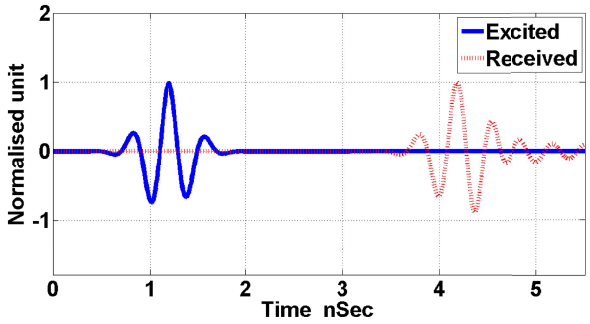

Fig. 6. Time domain performance of the antenna.

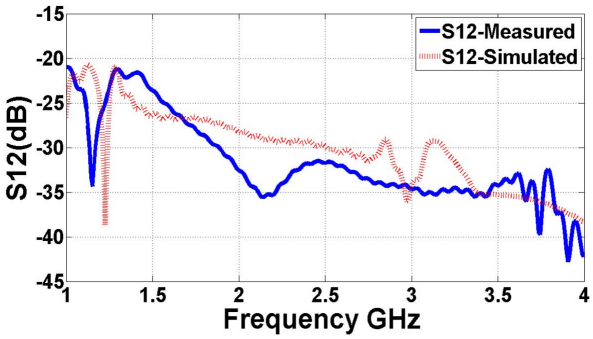

Fig. 7. Mutual coupling between a pair of neighboring antennas.

B. Platform

The platform is fabricated using polyvinyl-chloride (PVC). The platform has two plates; the lower one is designed to carry the head phantom. It has several adjustable rods to fix the phantom in place to avoid any movement that may cause an error in the measurements. The radius of that lower plate is 34 cm. The plate is marked to show the angle in deg steps with respect to the center. This is needed if the phantom is to be manually rotated.

To accommodate any reasonable head phantom size, the second plate has an inner radius of 17 cm and outer radius of 47 cm. It is mounted using eight poles that are adjustable in height in case there is a need to lower or lift the antenna array for different head phantoms or if a scanning of different head slices is needed. The plate has 16 slits for the antenna elements to be inserted and fixed in place. The plate also carries

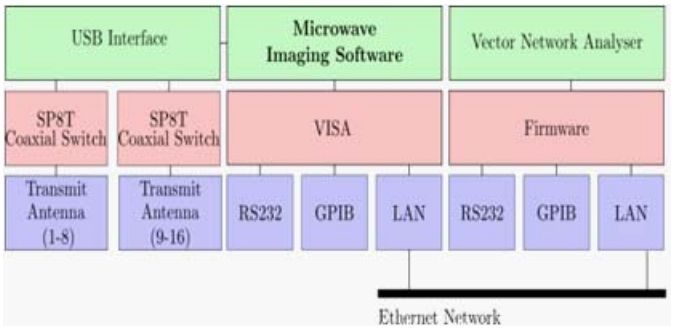

Fig. 8. Data collection procedure.

16 holders for the antenna elements. Those holders are adjustable horizontally in place so that the distance between the antenna elements and the phantom can be changed as required.

The designed platform can suit varieties of measurement configurations. This flexibility is necessary for the experimental assessment of a microwave imaging system. The height of the antenna array can be adjustable depending on the size of the phantom and the number of slicing for future 3-D imaging. In this paper, the horizontal distance between the antenna and the phantom to be imaged is kept at 0.5 cm.

C. Pulse Generation and Data Acquisition

The developed system uses the monostatic radar mode of operation. In this case, the same antenna elements are applied for transmitting and receiving the wideband signals. The signals are generated by the vector network analyser (VNA) in a step-frequency manner typically using 401 equidistant frequency points across the band from 1 GHz to 4 GHz. This operation is achieved using R&S ZVA24 VNA. Collecting the S-parameter data in a timely manner is important during operation of the microwave imaging system. This obviously requires an automated procedure between the computer running the microwave imaging software and the VNA.

With ZVA24 VNA, we use the virtual instrument software architecture (VISA): a standard for configuring and programming instrumentation via a variety of buses, such as GPIB, RS232, Ethernet, and USB [25]. Fig. 8 shows a system overview on the data collection procedure between the head imaging software and the VNA. As shown, we obtain the data via an Ethernet network which takes no more than three s to obtain 401 complex S-parameter measurements.

The transmitting antenna is selected by two single-pole eight-throw (SP8T) microwave, coaxial switches. One switch accesses elements 1–8 of the array, while the second switch accesses elements 9–16. The switches are toggled by a USB interface controlled by the microwave imaging software.

III. Imaging Algorithm

The transmission and reception of the excited signals are done at different spatial antenna locations and recorded in the frequency domain using the VNA. The received signal at the ith antenna, Γ_i is represented by a vector of 401 equidistant frequency points across the band from 1 GHz to 4 GHz. Γ_i is transformed into the positive-valued time domain vector ζ_i of 401 elements by applying inverse discrete Fourier transform IDFT as given by

$$\zeta_i = F^{-1}\Gamma_i \tag{1}$$

F^{-1} denotes $M \times M$ IDFT matrix with (n,k)th entry $1/Me^{j2\pi nk/M}$, where $M = 401$ and $i = 1, 2,.., N$. N denotes the size of antenna array resides in free-space along an elliptical trajectory at N discrete positions.

In this paper, a monostatic synthetic antenna aperture scheme is used where each antenna in the array sends sequentially a microwave signal with the wide spectrum (1–4 GHz) toward the head and captures the backscattered signal. Due to the heterogeneous structure of the head, a strong background reflection dominates the backscattered signals. The acquired signal at each antenna element is preprocessed to remove the common background reflections, such as the free space-head phantom interface reflections. Based on the anatomical symmetry of the head with respect to the central line that divides the head into left and right hemispheres, the background signals are expected to be almost identical. Therefore, the preprocessing is performed by subtracting the backscattered signals at antennas facing each other in the array with respect to the central line [26]

$$\Upsilon_i = \zeta_i - \zeta_j \tag{2}$$

$$\Upsilon_j = \zeta_j - \zeta_i = -\Upsilon_i \tag{3}$$

where $j = (N - i + 2) \bmod N$. Next, the negative parts of the constructed signals are chopped and replaced by zeros to avoid getting mirror images (ghosts) from the negative-time samples.

An imaging algorithm based on the confocal delay-and-sum algorithm is utilized for the post-processing of the determined target response at different time shifts. The confocal algorithms are applied extensively in ultrawideband breast imaging. The head H to be imaged is defined as a set of voxels of a dimension 0.5 mm × 0.5 mm with a center scattering point v. The outline of the head is defined by a series of boundary points β_i along the border circumference in Euclidean space defined by x and y coordinates $\{\beta_1$ (x, y), β_2 (x, y), β_3(x, y), …, $\beta_{\mathrm{NB}}(x, y)\}$.

To estimate the correct propagation path between each scattering point in the head domain and the transmitting antenna, Fermat's principle is implemented by constructing all possible propagation paths from the antenna to the boundary points, and then from the boundary points to the scattering point under test. For each $v_j \in$ H and antenna position S_k

$$d_i = \|S_k - \beta_i\| + \sqrt{\varepsilon}_{\mathrm{avg}} \left\|\beta_i - v_j\right\| \tag{4}$$

where $\varepsilon_{\mathrm{avg}}$ denotes the average permittivity of the main head tissues and it is taken here as 40. Accordingly the optimal path $d = \mathrm{argmin}[d_i]/i = 1, 2, \ldots NB$ is found. Based on the hypothesis of the propagation path, the time-delay τ of the spatial difference signals is determined by $2 * d/c$, where c is speed of light. Finally, the coherent summation of all the responses is performed to provide an image of backscattered signals' strength.

TABLE I
MATERIALS NEEDED TO FORM CSF, GREY MATTER, WHITE MATTER, AND HEMORRHAGIC STROKE (BLOOD)

	CSF	Grey	White	Blood
Water (mL)	150	570	364	100
Corn flour (g)	5.45	286	185	12.8
Gelatin (g)	0	0	9.8	24
Agar (g)	20.2	17.7	0	0
Sodium-azide (g)	0.15	0.57	0.36	0.1
Propylene glycol (g)	4	0	0	0

IV. HEAD PHANTOM

To test the designed system, a head phantom that includes the main tissues found in the human brain; skull, grey matter, white matter, and the cerebral spinal fluid (CSF) is fabricated. Mixtures that represent bleeding in the brain are also manufactured as this is a common sign of brain trauma.

In the imaging experiments, the bleeding-mimic mixtures can be included at any location in the phantom.

For a cost-effective phantom, the main components used to manufacture the proposed phantom are: water, corn flour, gelatin, agar, sodium azide, and propylene glycol as shown in Table I. In order to achieve a close match with the real brain tissues, the measured electrical properties of brain tissues reported in [27] and [28] are used as a guide to find the rate of mixing of the aforementioned materials to fabricate the tissues (CSF, grey matter, white matter, and blood). The dielectric probe HP85070 is used to measure the properties of the fabricated tissues and make sure of their close agreement (less than $\pm$ 5% difference) with the real values.

The procedure to form the phantom from the fabricated tissues is simple and fast. First, a skull made in the form of human head from polyvinyl chloride is used as a shell for this phantom. The cavity inside the skull is filled with materials that represent the CSF, grey matter, and white matter. To emulate the effect of the skin tissues, a 1 mm layer of glycerin and some chemical additives is used to cover the outside of the skull. For a final realistic shape for the head, and to create an environment that is as close as possible to reality, a wig is used to cover the head. Using our dielectric probe, the electrical properties of the wig and real human hair are measured and confirmed to have close values (average permittivity $\approx$2) across the band of interest in this paper. The fabricated head phantom is shown in Fig. 9.

V. RESULTS AND DISCUSSION

To test the capability of the designed system and imaging algorithms to detect brain injuries, an ellipsoidal target that emulates the properties of a hemorrhagic stroke is fabricated and inserted in different locations inside the head phantom. For a reasonable emulation of the size of brain area affected by that stroke, an ellipsoidal-shaped target is fabricated to have the diameters of 2 cm $\times$ 1 cm$\times$ 0.5 cm.

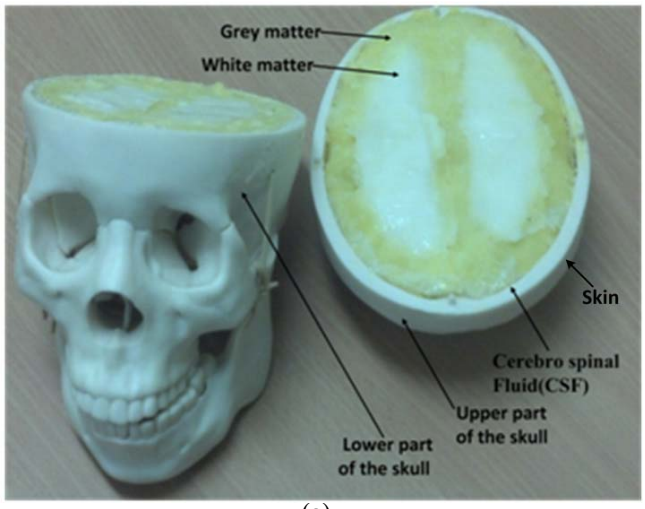

(a)

(b)

Fig. 9. (a) Tissues of the developed phantom. (b) Final developed phantom without and with a wig.

Before starting the imaging process, the system is calibrated over the desired frequency band from 1 GHz to 4 GHz. To that end, a modified one-port calibration procedure that involves three broadband standard loads is utilized. The standard coaxial short and shielded open circuits are used for the first two standard loads. This is the same as in the standard microwave calibration procedure. The third calibration standard is the load realized by the antenna radiating a microwave signal in free space. By using this calibration procedure, undesired signals, including internal reflections inside the antenna and at the antenna–air interface can be reduced or removed.

After the calibration, a stroke-affected head phantom is placed at the center of the platform. The controlling PC triggers the VNA to perform a number of measurement points (depending on the required specification) for reflection coefficients over the frequency band of interest. Complex, frequency-domain S-parameters are recorded at each of the 16 antennas. To investigate the effect of increasing the number of antennas to 32 without increasing the mutual coupling between them, the platform is rotated by an angle of 360/32 $=$ 11.25° after taking the measurements from the 16 elements. Another set of measurements is acquired. The combined two sets represent the case of using 32 antenna elements.

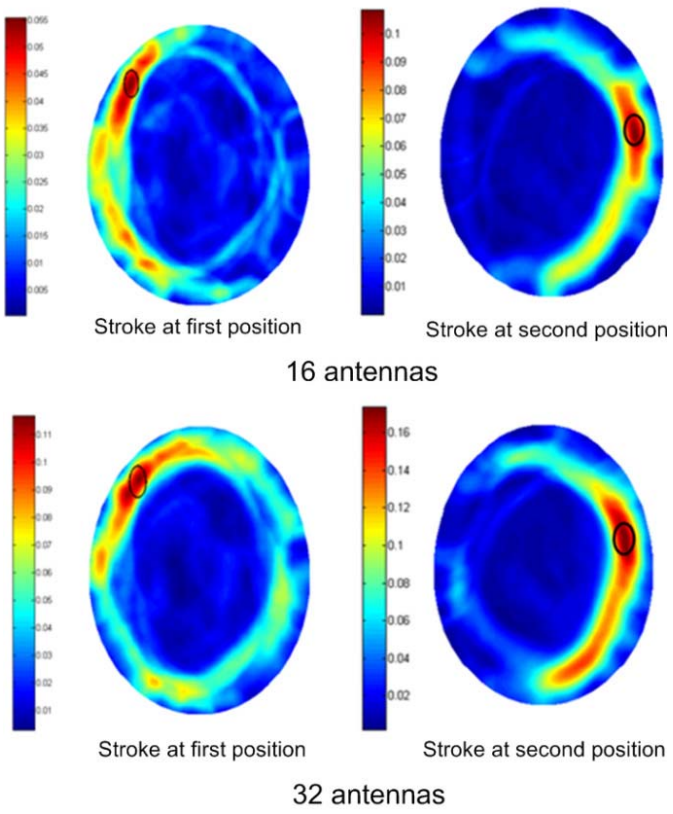

Fig. 10. Imaging results with two different locations of a hemorrhagic stroke. The exact locations of the strokes are indicated by black ellipses.

Subsequently, the aforementioned pre and post-processing algorithms are applied to get the desired 2-D image of the head phantom. The time needed to capture the S-parameters till getting the image is around 20 s using a standard desktop computer.

The obtained images are shown in Fig. 10 for two different realistic locations of the stroke. As the images portray, the stroke is clearly detected and localized for the two investigated cases. The accuracy of the results is higher with 32 antenna elements.

To quantify the efficacy of the imaging algorithm, the metric Δ is calculated from the obtained images. That metric defines the distance between the real center χ and the predicted center $\mathbf{p}^*$ of the target depending on the estimated maximum intensity, as given by

$$\Delta = \left\| \mathbf{p}^* - \chi \right\| \tag{5}$$

where $\mathbf{p}^* = \text{argmax}[I(\mathbf{p})]/\mathbf{p} \in \text{H}$. $\mathbf{I}(\mathbf{p})$ denotes the intensity of the discrete point $\mathbf{p}$, and H is the set of collected points that map the head area

For the images in Fig. 10, Δ is found to be 1 mm and 0.7 mm for the first position of a stroke using 16 and 32 antennas, respectively. Based on the second stroke position, Δ is found to be 5 mm and 1.5 mm using 16 and 32 antennas, respectively. Those results demonstrate the efficiency of the system to map the energy distribution in the head phantom. It accurately detects the existence of a stroke and predicts its location to within a few millimeters.

The proposed microwave imaging equipment can be applied to obtain images of different sections in the human brain. Those sections can then be combined, if needed, to form a 3-D image. Because of its low-cost, nonionization and hazard-free properties, the proposed system can be used frequently and continuously, which is an important advantage compared with conventional technologies such as X-ray, CAT or MRI. Furthermore, by being portable, it has the potential to offer new capabilities for medical personnel to provide an immediate diagnosis outside the hospital environment.

VI. Conclusion

A microwave system for head imaging was presented. The system utilized an array of 16 corrugated tapered slot antennas that operate across the band 1–4 GHz. A suitable switching device was used to enable the antennas to sequentially send microwave signals, whereas the backscattered signals were recorded in a vector network analyzer using the virtual instrument software architecture. To test the designed imaging system, a head phantom that emulates the electrical properties of real brain tissues with a hemorrhagic stroke was fabricated. A preprocessing algorithm that utilizes the symmetry of the two halves of human head was applied to extract the target response from the strong background reflections. A post-processing algorithm based on the confocal delay-and-sum approach was then used to accurately detect the existence and location of a hemorrhagic stroke inside the fabricated phantom.

Acknowledgment

The authors would like to acknowledge the efforts of K. Lane from the Mechanical Workshop, School of ITEE, The University of Queensland in the development of the imaging system's platform.

References

[1] I. T. Rekanos and T. D. Tsiboukis, "A finite element-based technique for microwave imaging of two-dimensional objects," *IEEE Trans. Instrum. Meas.*, vol. 49, no. 2, pp. 234–239, Apr. 2000.

[2] R. D. Monleone, M. Pastorino, J. Fortuny-Guasch, A. Salvade, T. Bartesaghi, G. Bozza, M. Maffongelli, A. Massimini, A. Carbonetti, and A. Randazzo, "Impact of background noise on dielectric reconstructions obtained by a prototype of microwave axial tomograph," *IEEE Trans. Instrum. Meas.*, vol. 61, no. 1, pp. 140–148, Jan. 2012.

[3] M. Benedetti, M. Donelli, A. Martini, M. Pastorino, A. Rosani, and A. Massa, "An innovative microwave-imaging technique for nondestructive evaluation: Applications to civil structures monitoring and biological bodies inspection," *IEEE Trans. Instrum. Meas.*, vol. 55, no. 6, pp. 1878–1884, Dec. 2006.

[4] A. Semnani, I. T. Rekanos, M. Kamyab, and T. G. Papadopoulos, "Two-dimensional microwave imaging based on hybrid scatterer representation and differential evolution," *IEEE Trans. Antennas Propag.*, vol. 58, no. 10, pp. 3289–3298, Oct. 2010.

[5] X. Zeng, A. Fhager, M. Persson, P. Linner, and H. Zirath, "Accuracy evaluation of ultrawideband time domain systems for microwave imaging," *IEEE Trans. Antennas Propag.*, vol. 59, no. 11, pp. 4279–4285, Nov. 2011.

[6] T. Henriksson, N. Joachimowicz, C. Conessa, and J. C. Bolomey, "Quantitative microwave imaging for breast cancer detection using a planar 2.45 GHz system," *IEEE Trans. Instrum. Meas.*, vol. 59, no. 10, pp. 2691–2699, Oct. 2010.

[7] M. Abou-Khousa, W. M. Saleh, and N. N. Qaddoumi, "Near-field microwave imaging utilizing tapered rectangular waveguides," *IEEE Trans. Instrum. Meas.*, vol. 55, no. 5, pp. 1752–1756, Oct. 2006.

[8] M. Chiappe and G. L. Gragnani, "Vivaldi antennas for microwave imaging: Theoretical analysis and design considerations," *IEEE Trans Instrum. Meas.*, vol. 55, no. 6, pp. 1885–1891, Dec. 2006.
[9] Z. Xuezhi, A. Fhager, P. Linner, M. Persson, and H. Zirath, "Experimental investigation of the accuracy of an ultrawideband time-domain microwave-tomographic system," *IEEE Trans. Instrum. Meas.*, vol. 60, no. 12, pp. 3939–3949, Dec. 2011.
[10] M. Ostadrahimi, P. Mojabi, S. Noghanian, L. Shafai, S. Pistorius, and J. LoVetri, "A novel microwave tomography system based on the scattering probe technique," *IEEE Trans. Instrum. Meas.*, vol. 61, no. 2, pp. 379–390, Feb. 2012.
[11] B. Mohammed, D. Ireland, and A. Abbosh, "Experimental investigations into detection of breast tumour using microwave system with planar array," *IET Microw. Antennas Propag.*, vol. 6, no. 12, pp. 1311–1317, Sep. 2012.
[12] S. Semenov and D. Corfield, "Microwave tomography for brain imaging: Feasibility assessment for stroke detection," *Int. J. Antennas Propag.*, vol. 2008, pp. 1–8, Mar. 2008.
[13] D. Ireland and M. Bialkowski, "Microwave head imaging for stroke detection," *Progr. Electromagn. Res.*, vol. 21, pp. 163–175, Oct. 2011.
[14] B. Mohammed, A. Abbosh, and D. Ireland, "Circular antenna array for brain imaging systems," in *Proc. IEEE Antennas Propag. Soc. Int. Symp.*, Chicago, IL, USA, Jul. 2012, pp. 1–2.
[15] B. Mohammed, A. Abbosh, and D. Ireland, "Stroke detection based on variations in reflection coefficients of wideband antennas," in *Proc. IEEE Antennas Propag. Soc. Int. Symp.*, Chicago, IL, USA, Jul. 2012, pp. 1–2.
[16] L. Catarinucci, P. Palazzari, and L. Tarricone, "On the use of numerical phantoms in the study of the human-antenna interaction problem," *IEEE Antennas Wireless Propag. Lett.*, vol. 2, no. 1, pp. 43–45, Feb. 2003.
[17] S. Mustafa, A. Abbosh, B. Henin, and D. Ireland, "Brain stroke detection using continuous wavelets transform matching filters," in *Proc. Int. Biomed. Eng. Conf.*, Cairo, Egypt, Dec. 2012, pp. 194–197.
[18] J. C. Lin and J. M. Clarke, "Microwave imaging of cerebral edema," *Proc. IEEE*, vol. 70, no. 5, pp. 523–524, May 1982.
[19] M. Sperandio, M. Guermandi, and R. Guerrieri, "A four-shell diffusion phantom of the head for electrical impedance tomography," *IEEE Trans. Biomed. Eng.*, vol. 59, no. 2, pp. 383–389, Feb. 2012.
[20] M. Akter, T. Hirai, Y. Hiai, M. Kitajima, M. Komi, R. Murakami, H. Fukuoka, A. Sasao, R. Tya, and E. M. Haacke, "Detection of hemorrhagic hypointense foci in the brain on susceptibility-weighted imaging: Clinical and phantom studies," *Acad. Radiol.*, vol. 14, no. 9, pp. 1011–1019, 2007.
[21] K. Karathanasis, I. Gouzouasis, I. Karanasiou, and N. Uzunoglu, "Experimental study of a hybrid microwave radiometry—Hyperthermia apparatus with the use of an anatomical head phantom," *IEEE Trans. Inf. Technol. Biomed.*, vol. 16, no. 2, pp. 241–247, Mar. 2012.
[22] B. Mohammed, A. Abbosh, B. Henin, and P. Sharpe, "Head phantom for testing microwave systems for head imaging," in *Proc. Int. Biomed. Eng. Conf.*, Cairo, Egypt, Dec. 2012, pp. 191–193.
[23] A. Abbosh, H. Kan, and M. Bialkowski, "Design of compact directive ultra wideband antipodal antenna," *Microw. Opt. Technol. Lett.*, vol. 48, no. 12, pp. 2448–2450, 2006.
[24] A. Abbosh, "Miniaturization of planar ultrawideband antenna via corrugation," *IEEE Antennas Wireless Propag. Lett.*, vol. 7, pp. 685–688, 2008.
[25] M. Bialkowski, D. Ireland, Y. Wang, and A. Abbosh, "Ultra-wideband array antenna system for breast imaging," in *Proc. Asia-Pacific Microw. Conf.*, Yokohama, Japan, 2010, pp. 267–270.
[26] S. Mustafa, B. Mohammed, and A. Abbosh, "Novel preprocessing techniques for accurate microwave imaging of human brain," *IEEE Antennas Wireless Propag. Lett.*, vol. 12, pp. 460–463, 2013.
[27] S. Gabriel, R. Lau, and C. Gabriel, "The dielectric properties of biological tissues: III. Parametric models for the dielectric spectrum of tissues," *Phys. Med. Biol.*, vol. 41, no. 11, pp. 2271–2293, 1996.
[28] C. Gabriel and S. Gabriel. (1996). *Compilation of the Dielectric Properties of Body Tissues at RF and Microwave Frequencies* [Online] Available: http://www.emfdosimetry.org/dielectric/Title/Title.html

Beada'a J. Mohammed received the B.Sc. and M.Sc. degrees in electrical engineering and electronics and communication engineering from Mosul University, Mosul, Iraq, in 1994 and 2002, respectively. She is currently pursuing the Ph.D. degree with the University of Queensland, Queensland, Australia.

Her current research interests include wideband antenna design and microwave imaging of human body.

Amin M. Abbosh (SM'08) received the M.Sc. degree in communication systems and the Ph.D. degree in microwave engineering from Mosul University, Mosul, Iraq, in 1991 and 1996, respectively, the Grad Cert in Higher Education from the University of Queensland, Queensland, Australia, in 2008, and the Doctor of Engineering degree from the University of Queensland in 2013.

He is currently the prestigious ARC Future Fellowship with the School of Information Technology and Electrical Engineering, University of Queensland. He has authored more than 200 papers on wideband passive microwave devices, planar antennas, and microwave-based imaging systems.

Samah Mustafa received the B.Sc. and M.Sc. degrees in electronic and communication engineering from Mosul University, Mosul, Iraq, in 1992 and 1998, respectively, and the Ph.D. degree in electronic and communication engineering from Baghdad University, Baghdad, Iraq, in 2004.

She was as a Visiting Lecturer with the Technical College and Technical Institute, Kirkuk, from 1992 to 1996. Since 1999, she has been an Academic Staff Member with the Electrical Department, College of Engineering Salahaddin University, Erbil, Iraq. She was a Visiting Academic with the University of California, Berkeley, CA, USA, from 2009 to 2010, and has been a Visiting Academic with the University of Queensland, Australia since 2012. Her current research interests include digital communication systems, signal processing, wireless network, and microwave imaging.

Dr. Samah was a recipient of the IWFF Award in 2009, the Endeavour Research Fellowship Award in 2012, and the FTFF Award in 2013.

David Ireland received the B.Eng. degree in microelectronic engineering from the Griffith University, Brisbane, Australia, in 2004, and the Ph.D. degree from Griffith University, Nathan, Australia, in 2010.

His current research interests include computational electromagnetics, microwave imaging, and stochastic optimisation. He was as a Research Fellow with the University of Queensland, Queensland, Australia, from 2010 to 2012. He is currently a Research Fellow with the Information and Communication Technologies Division, CSIRO, Queensland.